Phys. Status Solidi A **207**, No. 10, 2258–2262 (2010) / **DOI** 10.1002/pssa.201026048

physica status solidi a
www.pss-a.com
applications and materials science

# Carrier dynamics in InS nanowires grown via chemical vapor deposition

**Andreas Othonos*[,1] and Matthew Zervos[2]**

[1] Department of Physics, Research Centre of Ultrafast Science, University of Cyprus, P.O. Box 20537, 1678 Nicosia, Cyprus
[2] Department of Mechanical and Manufacturing Engineering, Nanostructured Materials & Devices Laboratory, Materials Science Group, University of Cyprus, P.O. Box 20537, 1678 Nicosia, Cyprus

Received 28 January 2010, revised 12 May 2010, accepted 28 May 2010
Published online 12 July 2010

**Keywords** InS, carrier dynamics, nanowires, time-correlating single photon counting, transient absorption spectroscopy

* Corresponding author: e-mail: othonos@ucy.ac.cy, www.ultrafast.ucy.ac.cy, Phone: +357 22 892827, Fax: +357 22 892821

Transient femtosecond absorption spectroscopy and time-correlating single photon counting (TCSPC) photoluminescence (PL) were employed to study InS nanowires (NWs) grown by chemical vapor deposition (CVD) and determine the relaxation mechanisms in these nanostructures. Intensity dependent measurements revealed that Auger recombination plays an important role in the relaxation of photogenerated carriers at fluences larger than $0.4 \times 10^{15}$ photons/cm$^2$. Calculations provided an estimated of the Auger recombination coefficient to be $1.1 \pm 0.5 \times 10^{-31}$ cm$^6$/s. At the low fluence regime TCSPC PL revealed three relaxation mechanisms with time constants ranging from ps to nanosecond providing evidence of the importance of non-radiative decay channels associated with defect/trap states within the NWs.

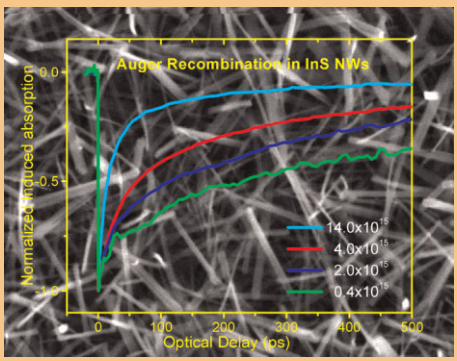


Auger recombination appears to dominate the carrier dynamics in InS NWs with increasing incident photon flux.



**1 Introduction** Indium sulfide ($In_xS_y$) has been receiving increasing attention as a chalcogenide semiconductor for its unique optoelectronic properties [1] and its application in second generation, thin film solar cells as an alternative to CdS and its intermediate band-gap of ~2.0–2.4 eV [2, 3]. $In_xS_y$ is a III–VI semiconductor and may exist in the cubic α-$In_2S_3$, tetragonal β-$In_2S_3$, trigonal γ-$In_2S_3$, or orthorhombic InS form [4]. Thin films of $In_xS_y$ have been grown so far by a variety of methods [5, 6] and most of them are actually polycrystalline, each having specific crystal, electrical, and optical properties depending on the growth method used.

In addition over the past few years there has been an up surging interest in one-dimensional nanostructures due to their intriguing properties [7–12] arising from their small size and high surface-to-volume ratio with potential applications in most areas of nanoscience and technology. Nanostructured $In_xS_y$ such as nanorods (NRs) [13], nanoparticles (NPs) [14], nanocrystals (NCs) [15, 16], nanowires (NWs) [17, 18] have been grown mainly by hydro or solvothermal [17, 19] and sol–gel [15, 16] methods which however are time consuming. Recently we demonstrated high yield-low temperature growth of InS NWs on Si(111) via the reaction of In and $InCl_3$ with $H_2S$ using atmospheric pressure chemical vapor deposition (APCVD) at 250 °C [20]. The InS NWs were found to self-assemble into urchin-like nanostructures at 300 °C while larger dandelion flowers and flat-hexagonal shaped crystals were obtained for growth temperatures ($T_G > 300$ °C) corresponding mainly to tetragonal β-$In_2S_3$. In addition to the growth of such NWs the study of their fundamental electronic and optoelectronic properties is indispensible for the development of nanoscale

devices such as third generation solar cells. Despite the potential applications of $In_xS_y$ NWs there has been no investigation into the fundamental carrier relaxation mechanisms of photogenerated carriers in this nanostructured material. Consequently here we investigate the carrier dynamics in $In_xS_y$ NWs and obtain a detail understanding of the various relaxation mechanisms and the influence of trap states using transient femtosecond (fs) absorption spectroscopy [21, 22] and time-correlated single photon photoluminescence (PL). Here we should point out that the NWs fabricated in this work are not electronically quantum confined since their diameter is much larger than the exciton Bohr radius and therefore their electronic band structure is likely very close to that of bulk material. However due to the large surface to bulk ratio we expect to observe some novel electronic and optical properties. For example, the large number of surface/trap states available makes carrier relaxation occur on a much faster time scale than in bulk material which may sometime inhibit relaxation mechanisms such as *photoluminescence* and *Auger recombination* [23].

**2 Results and discussion** InS NWs were grown using an APCVD reactor that consists of four mass flow controllers (MFCs) and a horizontal 1 in. diameter quartz tube furnace capable of reaching 1100 °C. For the purpose of optical measurements the $In_xS_y$ NWs were grown directly onto square pieces of quartz with an area of ≈7 $mm^2$ coated with Au that had a thickness of ≈1 nm. The morphology of the $In_xS_y$ NWs were examined with a TESCAN scanning electron microscope (SEM) while their crystal structure and the phase purity were confirmed using an X-ray diffractometer [20]. A typical example of the InS NWs obtained via the reaction of In and $InCl_3$ with $H_2S$ at $T_G = 250$–300 °C is shown in Fig. 1.

The InS NWs have an average length of 2 μm and diameters of 150 nm with a crystal structure corresponding to orthorhombic InS. The samples grown on quartz were carefully examined making sure that only NWs were present free from other structures or thin films. Thus measurements performed on the quartz samples provided information only on the NWs.

Following growth we carried out steady state optical transmission measurements from which we estimate the indirect energy band gap to be ≈2.4 eV. The weak absorption observed to persist for photon energies down to 1 eV is indicative of the existence of intermediate states within the band gap.

Steady state PL at room temperature (RT) of the InS NWs is shown in Fig. 2. The excitation was set far above the band gap at 4.1 eV (=300 nm) in order to cover a broad spectral range. The observed emission is very broad with the peak occurring around 420 nm. This PL maximum suggests that the most efficient emission occurs far above the indirect gap. In addition the broad spectrum suggests that emission occurs from a large number of energy states in these NWs mainly located above the energy band gap but also just below the conduction-band edge.

Furthermore, a contribution to the observed broad spectra may also be due to quantum confinement effects in the NWs. Here we should point out that the PL spectrum shown in Fig. 2 is very similar to the PL spectrum observed from the $In_2S_3$ nanofibers [18].

To further investigate the properties of these NWs and in particular the carrier relaxation mechanisms on a fs time scale we have utilized transient absorption [15] spectroscopy using pulse excitation at 3.1 eV. The experiments were carried out using a Ti: Sapphire ultrafast amplifier system generating 100 fs pulses at 800 nm and running at a repetition rate of 1 kHz. A nonlinear crystal was used to generate 400 nm for the purpose of exciting the NWs whereas part of the fundamental was used to generate a super continuum light for probing different energy states. Measurements were carried out using a typical pump–probe optical setup in a

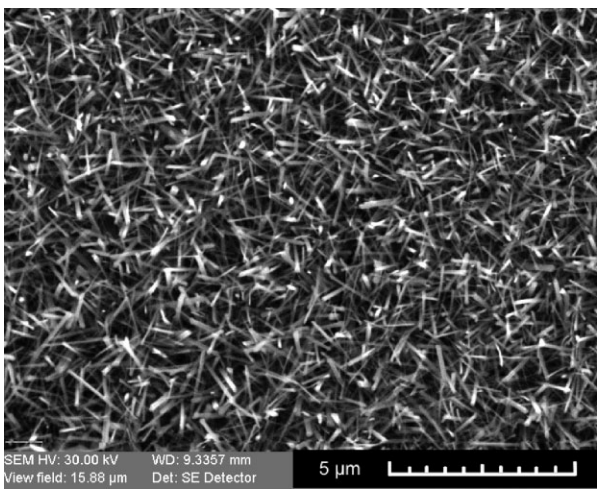


**Figure 1** SEM image of the InS NWs obtained via the reaction of In and $InCl_3$ with $H_2S$ at $T_G = 250$–300 °C.

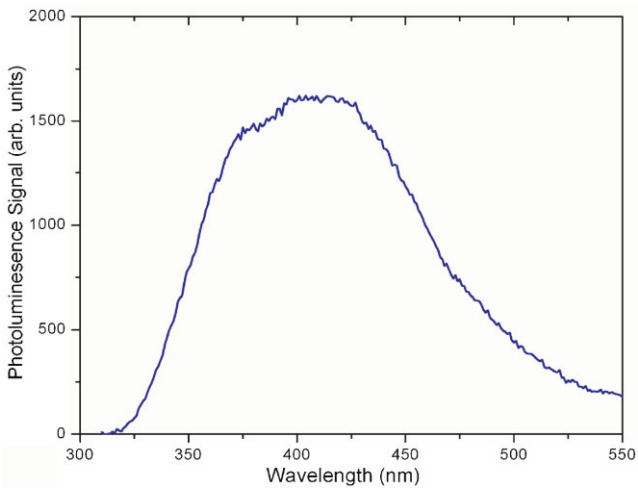


**Figure 2** (online color at: www.pss-a.com) Steady state room temperature photoluminescence spectrum of InS NWs grown on quartz and excited with a light source at 300 nm.

non-collinear configuration where differential reflection and transmission were utilized to determine the transient absorption. Figure 3 shows degenerate transient absorption measurements at 3.1 eV for various fluences corresponding to incident fluxes ranging from $0.4 \times 10^{15}$ up to $14 \times 10^{15}$ photons/cm$^2$. The inset shows the normalized transient absorption measurements for comparison.

The typical induced absorption has a sharp drop which is pulse width limited followed by a recovery which persists over a nanosecond time scale. Also evident from the normalized data is that the recovery toward equilibrium becomes faster with increasing incident absorption fluence. This negative induced absorption is due to what is normally referred to as "state filling." Following the generation of electrons and holes by the incident photons these photo-generated carriers will immediately occupy energy states that otherwise were available for absorption. Therefore probing these energy states will result in a reduction in the absorption due to the occupation of states. The occupied states become available once more due to energy relaxation resulting into a recovery of the absorption. This recovery provides a mean of observing the carrier energy relaxation in the InS NWs. The fact that carriers appear to return faster to their equilibrium state with increasing density of photo-generated carriers suggests that Auger recombination is a contributing factor in the relaxation of the excited carriers. Auger recombination appears to be negligible for incident fluence less than $0.4 \times 10^{15}$ photons/cm$^2$ which corresponds to an estimated carrier density of $3.6 \times 10^{19}$ carrier/cm$^3$. At this carrier density a best fit was obtained using a two exponential function with time constants of 20 ps (30%) and 650 ps (70%). The first time constant is probably associated with carrier relaxation into nearby energy states and possible surface/trap states, whereas the slower component is associated with relaxation of the carriers farther from the excitation region, most likely into traps within the band gap.

A more detailed analysis of the experimental data was performed using a simple differential equation model which incorporated the above two exponential decay mechanisms along with Auger recombination. Making use of the time constants obtained for the lowest fluence, where Auger recombination is considered negligible, it was possible to obtain fits to the differential absorption data at higher fluences. Relative good fits (Fig. 4) to all experimental data were obtained using an Auger coefficient of $1.1 \times 10^{-31}$ cm$^6$/s with a fitting error of $0.1 \times 10^{-31}$ cm$^6$/s whereas the error due to the uncertainty in the carrier density is much larger resulting in an error in the Auger coefficient of $\pm 0.5 \times 10^{-31}$ cm$^6$/s.

Here we should point out that non-degenerate transient absorption measurements covering the probing-spectral range between 500 and 900 nm reveal initial state filling associated with the occupation of the probed energy states following relaxation of the carriers generated by the 400 nm excitation pulse. The recovery of this state filling occurs within a few ps at which time "free carrier absorption" [22] becomes the dominant effect and persists over a few hundreds of ps where the carriers are captured by the various traps within the NWs. What is interesting to point out is that the effect of state filling is observed even when probing energy states located below the band edge of these NWs. Furthermore, the recovering of the state occupation appears to take longer at the lower lying energy states. Suggesting the photogenerated carries take longer time to redistribute them self in the various energy states/traps within the band gap.

To obtain a better understanding of the dynamics in the NWs on a longer time scale, time resolved PL were carried out using time-correlated single photon counting (TCSPC). The excitation was carried out using a 300 nm LED emitting

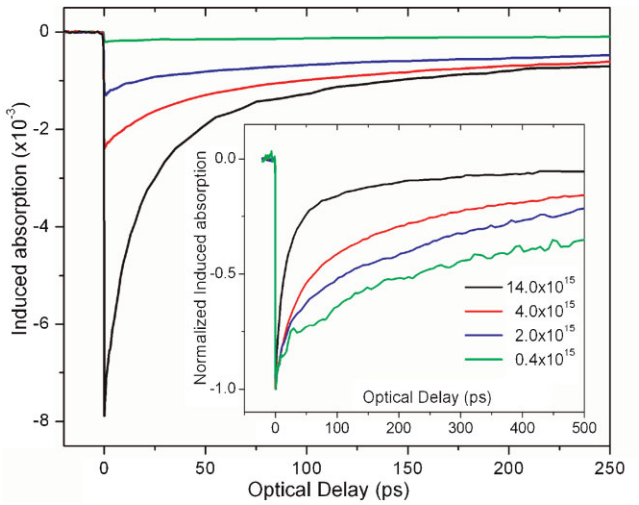


**Figure 3** (online color at: www.pss-a.com) Intensity dependent degenerate transient absorption data of the InS NWs at $\lambda = 400$ nm. The inset shows the same data normalized for comparison. The values in the legends correspond to the absorbed photons/cm$^2$.

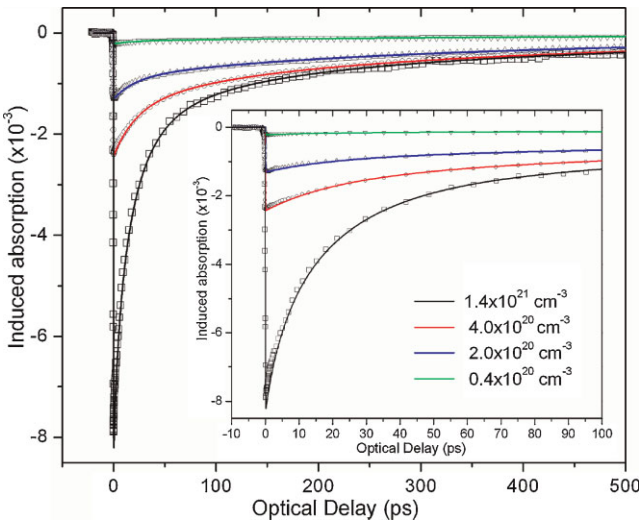


**Figure 4** (online color at: www.pss-a.com) Transient absorption data fitted with Auger coefficient of $1.1 \times 10^{-31}$ cm$^6$/s. The data are represented by symbols whereas the fitted curves by lines.

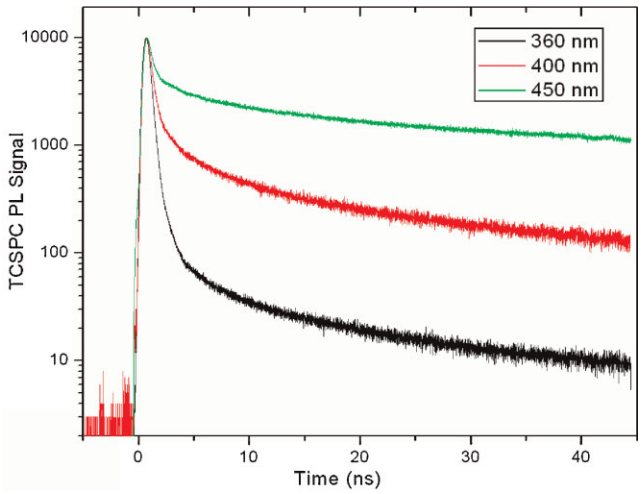


**Figure 5** (online color at: www.pss-a.com) Time-correlated single photon counting PL from InS NWs excited with a pulsed LED at 300 nm and probe at 360, 400, and 450 nm.

1 ns pulses with energy of 0.3 pJ/pulse at a repetition rate of 250 kHz. The spot size of the focused LED beam was ≈2 mm and generated a carried density which was several orders of magnitude smaller than the carrier density in the Auger regime seen in the fs experiments. A further reduction of the incident intensity using a neutral density filter in front of the LED revealed that the time constants were independent of the incident intensity. Figure 5 shows TCSPC data obtained at three different emission wavelengths namely at $\lambda = 360$, 400, and 450 nm over a time span of 45 ns. Clearly different decays profiles are obtained for the three probing wavelengths. Furthermore, analysis of the decay curves reveals that all profiles are well described by a tri-exponential function, i.e., $I(t) = A_1\,e^{-t/r_1} + A_2\,e^{-t/r_2} + A_3\,e^{-t/r_3}$, suggesting a complex energy level scheme structure for the InS NWs. The exponential time constants and their associated strengths are shown in Table 1. This tri-exponential decay of the PL signal indicates the existence of non-radiative channels available to the probing carriers. Although the measured PL signal comes from a particular energy state, the non-radiative channels available to the photogenerated carriers in these states alter the population thus making the PL decay appear multi-exponential. The fast time constant is thought to be associated with relaxation of the photogenerated carriers within the shallow traps, whereas the slower time constants are associated with the radiative recombination of carriers and the non-radiative recombination into the deep traps. It is important to point out that relaxation into the *shallow traps* appears to be most important for the higher lying energy states, as clearly seen at the 360 nm emission (93%) where the fast component is the dominant relaxation mechanism. Furthermore, for the lower lying energy states the radiative and non-radiative decay into *deep traps* becomes significant as seen at 450 nm. The important contribution of the non-radiative channels to the decay of the photogenerated carriers results in quenching the PL efficiency in the InS NWs.

**Table 1** Time constants from a tri-exponential fit of $I(t) = A_1\,e^{-t/r_1} + A_2\,e^{-t/r_2} + A_3\,e^{-t/r_3}$ to the curves of Fig. 5.

| $\lambda$ | 360 nm | | 400 nm | | 450 nm | |
|---|---|---|---|---|---|---|
| | $\tau_n$ (ns) | $A_n$ (%) | $\tau_n$ (ns) | $A_n$ (%) | $\tau_n$ (ns) | $A_n$ (%) |
| $n=1$ | 0.35 | 93 | 0.47 | 86 | 0.51 | 60 |
| $n=2$ | 2.34 | 4 | 4.40 | 10 | 5.70 | 18 |
| $n=3$ | 26.9 | 3 | 38.0 | 4 | 68.8 | 22 |

**3 Conclusions** We have investigated carrier dynamics of chemical vapor deposition (CVD) grown InS NWs using fs transient absorption spectroscopy and TCSPC PL. Degenerate pump probe intensity absorption measurements reveal state filling is the dominant effect with Auger recombination playing a major role in the relaxation dynamics of the photogenerated carriers for fluences larger than $0.4 \times 10^{15}$ photons/cm$^2$. The recovery of the induced absorption for the regime where Auger recombination is considered negligible revealed two relaxation mechanisms. Calculations using an estimate of the carriers generated in the InS NWs provided a value for the Auger coefficient of $1.1 \pm 0.5 \times 10^{-31}$ cm$^6$/s. TCSPC PL measurements for the low fluence regime at various probing wavelengths reveal different decay temporal profiles. A tri-exponential decay function was necessary to fit the data revealing two non-radiative channels for the carriers at the probing energy states in addition to the radiative one. At the higher lying states the main decay contribution comes from the non-radiative decay into the shallow trap states whereas at the lower lying states the decay into the deep trap states have also a sizable contribution. These non-radiative channels appear to quench the PL efficiency. Finally what is interesting to point out is that carrier dynamics in most NWs fabricated by present means are governed by the large number of surface states as well as other trap states energetically located within the bandgap of the material. As a result of these available relaxation channels carrier dynamics occur on a faster time scale than in bulk material inhibiting energy relaxation mechanisms such as PL.

**Acknowledgements** The work in this article was partially supported by the research programs; ERYAN/0506/04 and ERYNE/0506/02 funded by the Cyprus Research Promotion Foundation in Cyprus.

## References

[1] R. Nomura, S. Inazawa, K. Kanaya, and H. Matsuda, Appl. Organomet. Chem. **3**, 195 (1989).
[2] A. N. MacIness, W. M. Cleaver, R. Barron, M. B. Power, and A. F. Hepp, Adv. Mater. Opt. Electron. **1**, 229 (1992).
[3] N. Barreau, Sol. Energy **83**, 363 (2009).
[4] W. Rehwald and G. Harbeke, J. Phys. Chem. Solids **26**, 1309 (1965).

[5] N. A. Allsop, A. Schönmann, A. Belaidi, H.-J. Muffler, B. Mertesacker, W. Bohne, E. Strub, J. Röhrich, M. C. Lux-Steiner, and Ch.-H. Fischer, Thin Solid Films **513**, 52 (2006).
[6] M. Mathew, R. Jayakrishnan, P. M. R. Kumar, C. S. Kartha, and K. P. Vijayakumar, J. Appl. Phys. **100**, 033504 (2006).
[7] V. Klimov, P. Haring Bolivar, and H. Kurz, Phys. Rev. B **55**, 1463 (1996).
[8] V. I. Klimov and D. W. McBranch, Phys. Rev. B **55**, 173 (1997).
[9] R. D. Schaller and V. I. Klimov, Phys. Rev. Lett. **92**, 186601 (2004).
[10] J. C. Johnson, K. P. Knutsen, H. Yan, M. Law, Y. Zhang, P. Yang, and R. J. Saykally, Nano Lett. **4**, 197 (2004).
[11] R. P. Prasankumar, S. G. Choi, S. A. Trugman, S. T. Piraux, and A. J. Taylor, Nano Lett. **8**, 1619 (2008).
[12] R. P. Prasankumar, P. C. Upadhya, and A. J. Taylor, Phys. Status Solidi B **246**, 1973 (2009).
[13] A. Datta, S. K. Panda, S. Gorai, D. Ganguli, and S. Chaudhuri, Mater. Res. Bull. **43**, 983 (2008).
[14] D. P. Dutta, G. Sharma, A. K. Tyagi, and S. K. Kulshreshtha, Mater. Sci. Eng. B **138**, 60 (2007).
[15] W. Han, L. Yi, N. Zhao, A. Tang, M. Gao, and Z. Tang, J. Am. Chem. **130**, 13152 (2008).
[16] A. Datta, S. Gorai, and S. Chaudhuri, J. Nanopart. Res. **8**, 919 (2006).
[17] A. Datta, S. Gorai, S. K. Panda, and S. Chaudhuri, Gryst. Growth Des. **6**, 1010 (2006).
[18] X. Zhu, J. Ma, Y. Wang, J. Tao, J. Zhou, Z. Zhao, L. Xie, and H. Tian, Mater. Res. Bull. **41**, 1584 (2006).
[19] S. D. Naik, T. C. Jagadale, S. K. Apte, R. S. Sonawane, M. V. Kulkarni, S. I. Patil, S. B. Ogale, and B. B. Kale, Chem. Phys. Lett. **452**, 301 (2008).
[20] M. Zervos, P. Papageorgiou, and A. Othonos, J. Cryst. Growth **312**, 656 (2010).
[21] A. Othonos, J. Appl. Phys. **83**, 1789 (1998).
[22] A. Othonos, M. Zervos, and M. Pervolaraki, Nanoscale Res. Lett. **4**, 122 (2009).
[23] A. Othonos, E. Lioudakis, and A. G. Nassiopoulou, Nanoscale Res. Lett. **3**, 315 (2008).

 